Net synaptic drive of fast-spiking interneurons is inverted towards inhibition in human FCD I epilepsy

Eunhye Cho [1,2], Jii Kwon [2], Gyuwon Lee [2], Jiwoo Shin [1,2], Hyunsu Lee [3], Suk-Ho Lee [1,2], Chun Kee Chung [4,5,*], Jaeyoung Yoon [1,6,*], Won-Kyung Ho [1,2,*]

Author affiliations:

[1] Cell Physiology Laboratory, Department of Physiology, Seoul National University College of Medicine

[2] Department of Brain and Cognitive Sciences, Seoul National University College of Natural Sciences

[3] Department of Physiology, Pusan National University School of Medicine

[4] Department of Neurosurgery, Seoul National University Hospital

[5] Neuroscience Research Institute, Seoul National University Medical Research Center

[6] Present address: F.M. Kirby Neurobiology Center, Boston Children's Hospital, Harvard Medical School

* Corresponding authors

Corresponding authors:

Won-Kyung Ho

Department of Physiology, Seoul National University College of Medicine, 103 Daehak-ro, Jongno-gu, Seoul 03080, Republic of Korea.

wonkyung@snu.ac.kr

Jaeyoung Yoon

F.M. Kirby Neurobiology Center, Boston Children's Hospital, Harvard Medical School, 3 Blackfan St. CLS 13030.15, Boston, MA 02115, USA.

jy.yoon@tch.harvard.edu

Chun Kee Chung

Neuroscience Research Institute, Seoul National University Medical Research Center, 103 Daehak-ro, Jongno-gu, Seoul 03080, Republic of Korea.

chungc@snu.ac.kr

32

Abstract

Focal cortical dysplasia type I (FCD I) is the most common cause of pharmaco-resistant epilepsy with the poorest prognosis. To understand the epileptogenic mechanisms of FCD I, we obtained tissue resected from patients with FCD I epilepsy, and from tumor patients as control. Using whole-cell patch clamp in acute human brain slices, we investigated the cellular properties of fast-spiking interneurons (FSIN) and pyramidal neurons (PN) within the ictal onset zone. In FCD I epilepsy, FSINs exhibited lower firing rates from slower repolarization and action potential broadening, while PNs had increased firing. Importantly, excitatory synaptic drive of FSINs increased progressively with the scale of cortical activation as a general property across species, but this relationship was inverted towards net inhibition in FCD I epilepsy. Further comparison with intracranial electroencephalography (iEEG) from the same patients revealed that the spatial extent of pathological high-frequency oscillations (pHFOs) was associated with synaptic events at FSINs.

Introduction

Epilepsy is a disorder characterized by recurrent seizure episodes.[1,2] Approximately 50 million people suffer from epilepsy, more than a quarter of which are pharmaco-resistant.[3,4] Focal cortical dysplasia (FCD) is the most common pathology associated with pharmaco-resistant epilepsy, which requires surgery to alleviate symptoms.[5] FCD is categorized into three types: type I is characterized by abnormalities in cortical lamination, while type II further introduces neuronal dysmorphisms; when type I FCD is associated with heterogeneous brain lesions, it is classified as type III.[6-8] For FCD II pathogenesis, single causative genetic mutations in the mammalian target of rapamycin (mTOR) pathway have been identified.[9,10] However, the genetic background and epileptogenic mechanisms remain unknown for FCD I,[11,12] despite the poorer postoperative seizure-free outcome (Engel class I at 5 years: 54.5% vs. 67.4%).[13,14]

Excitation-inhibition (E-I) balance is a fundamental feature of the cortical network. The cortical network can remain robust to modest perturbations because of the E-I balance maintained by recurrent local activity.[15,16] Since the defining feature of seizure is the uncontrolled burst of electrical activity, disruption in the E-I balance from reduced inhibition has been considered the main candidate cause of epileptogenesis. In support of this hypothesis, pyramidal neurons (PNs) within the ictal onset zone were found to receive less spontaneous inhibitory postsynaptic currents,[17-19] and a decrease in the number of parvalbumin-expressing interneurons (PVINs)[20-22] or $GABA_A$ receptor conductance and expression on PNs[23] have been observed. However, these studies did not specifically address FCD I, even though epileptogenic mechanisms are expected to be distinct for each type of FCD.

Intracranial electroencephalography (iEEG) from epilepsy patients revealed that pathological high-frequency oscillations (pHFOs) were increased in epileptic regions.[24,25] pHFOs are

defined as ripples (80-200 Hz) or fast ripples (200-500 Hz) that are distinguished from physiological HFOs by frequent association with spikes or pathological slowing.[26] Since the resection of tissue exhibiting pHFOs has been found to be closely linked to the success of epilepsy surgery,[27-29] it is of great interest to investigate the relationship between epileptogenic mechanisms and the occurrence of pHFOs. Previous studies suggested a potential role of fast-spiking interneurons (FSINs), which represent a largely overlapping population with PVINs, in the generation of pHFOs possibly by causing out-of-phase or asynchronous firing of PNs.[30-32] Still, a comprehensive understanding of changes in FSIN physiology and cortical E-I balance underlying pHFO generation remains elusive despite the growing clinical significance of pHFOs.

To understand the cellular mechanisms of FCD I epileptogenesis, we investigated the electrophysiological properties of human FSINs and PNs using whole-cell patch clamp in acute human brain slices. We prioritized neocortical layer 2/3 (L2/3) where pathological phenotypes of FCD I are the most prominent.[33,34] Then, the clinical significance of these cellular properties was examined through correlative analysis with the spatiotemporal characteristics of pHFOs in iEEG recorded from the same patients. We found that both the intrinsic and synaptic excitability of FSINs were reduced in FCD I epilepsy. In the non-epileptic control, synaptic excitation-to-inhibition ratio at FSINs increased as more inputs were activated simultaneously, suggesting a progressively important role of FSINs in stabilizing the network under high-activity state. Such pattern of E-I balance at FSINs was preserved across species in non-epileptic conditions, but disrupted in FCD I epilepsy in the form of net inhibition of FSINs. Furthermore, we found that the spatial extent of cortical areas exhibiting ictal discharges or pHFOs was most closely related to spontaneous synaptic activity at FSINs, while pHFO occurrence could be explained by PN firing rate. We conclude that the shift in net synaptic drive at FSINs from excitation to inhibition represents the major epileptogenic mechanism of

FCD I epilepsy, highlighting the pathophysiological significance of FSINs in relation to cortical E-I balance.

Results

To determine changes in the intrinsic neuronal excitability and synaptic E-I balance leading to FCD I epileptogenesis, we obtained neocortical tissue containing the ictal onset zone surgically resected from 15 patients with intractable epilepsy diagnosed with FCD I or III (FCD I accompanied by heterogenous lesions). In addition, we obtained non-pathological parts of the neocortex resected from 10 tumor patients without seizure history as a control (Supplementary Table 1). Using whole-cell patch clamp in acute human brain slices, we examined the electrophysiological properties of FSINs and PNs in neocortical L2/3.

Human L2/3 FSINs in FCD I epilepsy have decreased firing due to action potential broadening

A major contributor to cortical network hyperactivity is the decrease in the number of GABAergic interneurons or their effectiveness in inhibiting excitatory neurons,[20-23] but the cellular phenotypes of decreased inhibition have not been identified in detail. Hence, we first examined the intrinsic excitability of FSINs in control and epileptic conditions (Fig. 1a). The resting membrane potential (RMP) and input resistance (R_{in}) of FSINs were not significantly different between control and FCD I epilepsy (Fig. 1b-c). FSINs in FCD I epilepsy, however, exhibited pronounced differences in their firing properties, resulting in firing rates that were

lower by up to 40% compared to control (171.8 vs. 103.9 Hz; Fig. 1d). Analysis of single action potential (AP) kinetics further revealed that the AP duration of FSINs was considerably longer in FCD I epilepsy due to slower depolarization and repolarization, while AP threshold was unaffected (Supplementary Fig. S1).

Similarly, we compared the intrinsic excitability of PNs between control and epileptic conditions (Fig. 1e). For PNs, RMP was not different between groups (Fig. 1f), but R_{in} was significantly higher in FCD I epilepsy (109.4 vs. 156.7 MΩ; Fig. 1g). While RMP and R_{in} of human L2/3 PNs had been found to be correlated with cortical depth,[35] here it was not a contributing factor as cortical depths were not significantly different between groups (Supplementary Fig. S2). In alignment with increased R_{in}, PNs in epilepsy exhibited higher firing frequency in response to smaller somatic current injection (5.6 vs. 10.1 Hz at 150 pA); however, firing rates saturated towards a similar value at larger current amplitudes (Fig. 1h).

To understand the mechanisms underlying changes in FSIN and PN firing rates in FCD I epilepsy, we analyzed their correlations with single AP kinetics and found a significant relationship between FSIN firing rate and AP half-width (Fig. 1i), and in turn between AP half-width and the maximum rate of repolarization (Fig. 1j), from FSINs in both control and FCD I epilepsy. On the other hand, PN firing rate was not correlated with single AP kinetics, but instead strongly correlated with R_{in} (Fig. 1k), implying that the higher firing rates of PNs may not be attributable to changes in the dynamic properties of ion channels but to increased R_{in}. Taken together, these results suggest that the major mechanisms determining the firing output of FSINs and PNs are distinct, and differently affected by FCD I epilepsy.

Synaptic conductance from spontaneous events is biased towards inhibition in both FSINs and PNs

We hypothesized that differences in the intrinsic excitability of single neurons in FCD I epilepsy would be accompanied by changes in synaptic properties, which may have more prominent consequences towards network hyperexcitability. To this end, we first measured the spontaneous excitatory and inhibitory postsynaptic currents (sEPSC and sIPSC) at FSINs and PNs. At postsynaptic FSINs (Fig. 2a), sEPSC but not sIPSC frequency was higher (Fig. 2b), while both sEPSC and sIPSC amplitudes were larger (Fig. 2c), in FCD I epilepsy compared to control. For quantitative comparison of synaptic strengths, we converted the excitatory and inhibitory postsynaptic current amplitudes to conductances (G_E and G_I; see Methods) and found that the spontaneous inhibitory conductance ($G_{I,s}$) was higher than the spontaneous excitatory conductance ($G_{E,s}$) at FSINs, in both control and FCD I epilepsy (Fig. 2d). However, the E-I ratio of spontaneous postsynaptic conductances ($G_{E,s}/G_{I,s}$) remained at approximately 0.6 for both groups, indicating that the increase in $G_{E,s}$ in FCD I epilepsy occurred in parallel with the increase in $G_{I,s}$ (Fig. 2e). Spontaneous synaptic events at PNs followed a qualitatively similar pattern (Fig. 2f). While sEPSC and sIPSC frequencies were unchanged (Fig. 2g), sEPSC amplitude was larger in FCD I epilepsy (Fig. 2h); sIPSC amplitude was also nominally larger, but without statistical significance (23.2 vs. 28.0 pA, P = 0.069). $G_{I,s}$ was larger than $G_{E,s}$ by more than twofold in both control and epilepsy (Fig. 2i), resulting in a lower $G_{E,s}/G_{I,s}$ of 0.4 at PNs from both groups (Fig. 2j). These results show that spontaneous excitatory and inhibitory conductances were amplified at both FSINs and PNs in FCD I epilepsy, but to similar extents such that their ratio was preserved, with larger inhibitory component.

Synaptic excitability of FSINs increases progressively with the scale of cortical activation, but not in FCD I epilepsy

To specifically examine postsynaptic responses to presynaptic AP firing, we then measured the evoked excitatory and inhibitory postsynaptic currents (eEPSC and eIPSC) in response to local electric stimulation in L2/3 (Fig. 3a). To obtain putative single synaptic responses, we used a conventional minimal stimulation approach as has been established previously (see Methods). eEPSC and eIPSC from minimal stimulation are referred to as $eEPSC_{min}$ and $eIPSC_{min}$ (Fig. 3a, lighter traces). Additionally, we measured postsynaptic responses evoked by activation of a larger cortical volume, intended for simultaneous recruitment of the maximal number of afferents converging onto the postsynaptic neuron (Fig. 3a, darker traces). For this purpose, we elected a stimulation protocol at which intensity the eEPSC amplitude reached a plateau (Supplementary Fig. S3; see Methods); since both the electric field from a monopolar current source as well as its effect on membrane potential are linearly proportional to current amplitude and inversely proportional to distance,[36-38] saturation of eEPSC amplitude can be expected to result from the activation of the maximal number of presynaptic connections arriving at the postsynaptic neuron. Subsequently, eEPSC and eIPSC produced by these stimulation conditions were regarded as maximally evoked responses, henceforth referred to as $eEPSC_{max}$ and $eIPSC_{max}$. Peak amplitudes of these events were determined predominantly by monosynaptic inputs, as evidenced by their short latencies that were not different from those of single synaptic events from minimal stimulation (Supplementary Fig. S4).

At FSINs in control conditions, we found that the excitatory conductance calculated from the postsynaptic current amplitude in response to minimal stimulation ($G_{E,min}$) was no longer smaller than the corresponding inhibitory conductance ($G_{I,min}$) (Fig. 3b), unlike those from spontaneous events. The trend of increasing excitatory synaptic conductance was stronger with large-scale stimulation, at which point the excitatory conductance ($G_{E,max}$) had exceeded the

inhibitory postsynaptic conductance ($G_{I,max}$) (Fig. 3c). In contrast, $G_{E,min}$ and $G_{E,max}$ at FSINs in FCD I epilepsy were accompanied by larger $G_{I,min}$ and $G_{I,max}$ compared to control (Fig. 3b-c). When the changes in G_E and G_I in response to increasing stimulation were plotted against each other, it became clear that FSINs in control conditions grew progressively more excitable synaptically with larger scale cortical activation, whereas in FCD I epilepsy, inhibition was dominant over excitation regardless of the scale of stimulation (Fig. 3d, Supplementary Fig. S5). E-I ratio of postsynaptic conductances (G_E/G_I) at control FSINs therefore increased gradually from below 1 (net inhibition) with spontaneous inputs to increasingly larger values above 1 (net excitation) with synaptic activation, while G_E/G_I remained below 1 at FSINs in FCD I epilepsy (Fig. 3e).

To further understand the mechanisms underlying this difference, we used the fold changes in synaptic conductance introduced by increasing the stimulation scale as a metric to represent functional connectivity, given that minimal or maximal stimulation respectively represents single synaptic events or the collective activation of synaptic afferents. Based on this criterion, excitatory connectivity at postsynaptic FSINs (represented by $G_{E,max}/G_{E,min}$) was reduced by 55% in FCD I epilepsy, while the change in inhibitory connectivity (represented by $G_{I,max}/G_{I,min}$) was nonsignificant (Fig. 3f). Excitatory connectivity at postsynaptic FSINs was substantially higher than inhibitory connectivity, consistent with known architecture of the human cortex that connection probability between those two synapse types is similar, but the total number of excitatory connections greatly outnumber that of inhibitory connections.[39] Our findings demonstrate that synaptic E-I balance at FSINs under normal conditions is characterized by an increasing net excitatory synaptic drive in response to increased cortical activation owing to higher excitatory synaptic connectivity compared to inhibitory connectivity, but this property is inverted towards net inhibition of FSINs in FCD I epilepsy due to reduced excitatory connectivity.

Synaptic E-I relationship is conserved across species

Synaptic excitation was gradually favored over inhibition at FSINs with increasing stimulation, but only in non-epileptic conditions and not FCD I epilepsy (Fig. 3d-e). To investigate whether this E-I relationship of synaptic conductances represented a general characteristic of cortical networks, we repeated analogous experiments in the rat temporal association cortex (TeA) for cross-species comparison (Fig. 3g). In rat FSINs, sEPSC was smaller than sIPSC, but $eEPSC_{min}$ was similar to $eIPSC_{min}$, and $eEPSC_{max}$ was larger than $eIPSC_{max}$; accordingly, G_E grew progressively larger than G_I with increasing synaptic activation (Fig. 3h). Consequently, G_E/G_I at rat FSINs evolved along a strikingly similar pattern compared to FSINs in the non-epileptic human cortex (Fig. 3i-j). These findings confirm that the relationship between excitatory and inhibitory synaptic conductances at FSINs, namely the preferential recruitment of excitatory inputs upon larger scale cortical activation to overcome the initial inhibition dominance, represents a general characteristic of cortical E-I balance conserved across species.

Network hyperactivity in FCD I epilepsy is mediated mainly by FSINs, while monosynaptic E-I relationship at PNs is unaffected

We then continued to compare the excitatory and inhibitory synaptic conductances at PNs (Fig. 4a). From minimal stimulation, $G_{E,min}$ was higher in FCD I epilepsy compared to control (0.3 vs. 0.8 nS, P = 0.0040; Fig. 4b), but $G_{E,min}$ was not significantly different from $G_{I,min}$, in both control and FCD I epilepsy. Similarly, $G_{E,max}$ from maximal stimulation was also comparable to $G_{I,max}$ (Fig. 4c). Nevertheless, a quantitatively similar shift towards stronger excitation in FCD I epilepsy was noticeable from both conditions in terms of G_E/G_I ($G_{E,min}/G_{I,min}$, 0.5 vs.

0.8; $G_{E,max}/G_{I,max}$, 0.5 vs. 0.7). In contrast to FSINs, the E-I ratio of G_E/G_I was always below 1 at PNs (Fig. 4d); in other words, net postsynaptic conductance at PNs always favored inhibition regardless of synaptic activation scale, in both control and FCD I epilepsy. The synaptic E-I relationship at PNs was again not different between the non-epileptic human cortex and the rat cortex, further confirming that this represented a conserved pattern of cortical E-I balance (Supplementary Fig. S6). These results show that monosynaptic E-I relationship at PNs is relatively less affected in FCD I epilepsy, and net synaptic conductance at PNs remains biased towards inhibition regardless of cortical activation scale.

For a numerical representation of network excitability using simpler variables compatible with recurrent network models,[40] we defined the synaptic excitability variable $G = (G_{EE} \cdot G_{II})/(G_{EI} \cdot G_{IE})$, where G_{XY} denotes synaptic conductance from presynaptic population Y to postsynaptic population X, and X, Y $\in$ {E, I};[41] in other words, G is equal to G_E/G_I at PNs divided by G_E/G_I at FSINs. At the network level, FSINs were preferentially recruited during progressively higher cortical activity state in control conditions, but not in FCD I epilepsy. Specifically, G_E/G_I at PNs was lower than the G_E/G_I at FSINs in the non-epileptic control due to the progressive increase in the latter (Fig. 4e), but this relationship was inverted in FCD I epilepsy with stimulation (Fig. 4f), such that the synaptic excitability variable G decreased with larger scale cortical activation in the non-epileptic control but instead increased in FCD I epilepsy (Fig. 4g). Notably, such divergence in terms of synaptic excitability was not observed with spontaneous activity alone, suggesting that it was imparted by changes in functional connectivity. Collectively, our results indicate that a decrease in both the intrinsic and the synaptic excitability of FSINs, accompanied additionally by the increase in the R_{in} of PNs, introduces a shift in the E-I balance towards an overall elevation of cortical activity state in FCD I epilepsy.

Clinical presentation of pathological iEEG activity is associated with spontaneous synaptic activity at FSINs

pHFOs representing synchronized neuronal activity have been used as a marker for epileptic discharges.[30-32] To find potential clinical implications of our findings, we thus investigated whether the intrinsic and synaptic properties of neurons in FCD I epilepsy that we obtained with ex vivo electrophysiology were associated with the characteristics of pHFOs. We estimated the extent of cortical area involved in epileptogenesis by counting the number of channels that exhibited either ictal discharges or pHFOs from each patient (Fig. 5a). Then, these single-cell and extracellular properties were compared using Pearson and Spearman correlations (Supplementary Fig. S7-S8); correlations were considered significant when both coefficients met the criteria (see Methods). The spatial extent of cortical areas presenting pathological iEEG activity (ictal/pHFO area) varied across patients (Fig. 5b; Supplementary Fig. S9). We found that ictal/pHFO area was positively correlated with both the frequency and the amplitude of sEPSC at postsynaptic FSINs (Fig. 5c-e). Although sIPSC amplitude had no correlation with ictal/pHFO area, the strongest correlations were found between ictal/pHFO area and sIPSC frequency at either FSINs or PNs (Fig. 5f-h), both of which can be expected to reflect presynaptic FSIN activity as inhibitory inputs onto postsynaptic FSINs are known to originate mostly from other FSINs, in humans as well as rodents.[39,42] These results imply that spontaneous synaptic activity at FSINs contributes to the spatial characteristics of pHFOs at resting state, considering that these iEEG signals were obtained during a stable resting state (see Methods).

pHFO occurrence is associated with higher PN firing rate

Finally, we examined whether the propensity of pHFO occurrence was likewise correlated with the cellular properties measured from ex vivo experiments. For this purpose, we counted ripple and fast ripple pHFOs separately from a 1-hour monitoring period (Fig. 6a-b; see Methods) and analyzed their correlations with the same intrinsic and synaptic properties. Similar to ictal/pHFO area, pHFO occurrence varied across patients (Fig. 6c-d). We did not find an otherwise inherent tendency for pHFO occurrence aside from patient-to-patient variability, as there was no noticeable bias in the distribution of pHFO occurrences when all channels were collected irrespective of patient (Fig. 6e-f). Unlike ictal/pHFO area which was correlated with spontaneous synaptic events, pHFO occurrence, averaged across channels displaying pHFOs per patient, showed positive correlations with PN firing frequency for both ripple and fast ripple pHFOs (Fig. 6g-i). These results suggest that, while synaptic changes in FCD I epilepsy involving FSINs contribute the most to the spatial extent of pathological activity, the generation of pHFOs is more closely related to the increased intrinsic excitability of PNs. We note, however, that considering their association had to be limited to correlative measures as these data originated from two dissociated conditions of ex vivo and in vivo, and further study in the scope of clinical research is thus required to ascertain a causal link between these candidate cellular mechanisms and epileptic activity observed in patients.

Discussion

Our understanding of epileptogenesis hinges on intrinsic, synaptic, and glial factors.[43] Recent advances have begun to reveal the potential link between aberrant molecular pathways and

hyperexcitability in the dysplastic cortex.[44] However, these discoveries were centered on FCD II, while epileptogenic mechanisms remain largely unknown for FCD I which is more common but less successfully treated. In a recent study using a mouse model of FCD II, hyperexcitability was found to originate not from the neurons carrying somatic mTOR mutations but instead from nearby non-mutated neurons. More importantly, synaptic E-I balance was unchanged in this model of FCD II.[45] From histological examinations, a reduction in PV immunoreactivity was observed from FCD I, but not FCD II.[22] In addition, the temporal characteristics of the interictal epileptiform discharge and the repetitive discharge in iEEG were found to be sufficiently distinct between FCD I and FCD II such that the underlying FCD type can be reliably predicted.[46] These results strongly suggest that epileptogenic mechanisms are specific to the type of associated FCD, of which FCD I is poorly understood.

In the present study, we examined the electrophysiological properties of PNs and FSINs in the adult human cortex to investigate the epileptogenic mechanisms in FCD I. Empirical knowledge from acute human brain slices regarding synaptic physiology in addition to intrinsic membrane properties are scarce.[39,47-54] Moreover, these studies often used tissue outside of the ictal zone, with the specific intent to explore normal physiology unrelated to seizure activity. We instead set our focus to the pathophysiology of FCD I epilepsy by conducting experiments from within the seizure onset zone. The findings from the epileptic cortex were then compared with those from the control cortex unassociated with epilepsy. Notably, the intrinsic properties of neurons in these epileptic areas contrasted those from parts of the cortex that were obtained from epilepsy patients but instead clinically categorized as nonpathological, with cortical tissue from tumor patients as a control in both cases.[54] All of our recordings were made from L2/3; while a more comprehensive perspective incorporating the entire cortical column would be ideal, it is beyond the scope of the current study as very little is known about translaminar interactions or connectivity. Nonetheless, the choice of L2/3 is appropriate considering that the

pathological phenotypes of FCD I are the most severe in supragranular layers.[33,34] Moreover, cortical expansion has evolved in such way that the relative thickness of supragranular layers that contain the majority of intracortical connections is largest in humans and other primates, unlike the rodent cortex in which infragranular layers are thicker.[55-58]

Since FSINs are the primary regulators of cortical network excitability, abnormal development or function of FSINs have been implicated with epilepsy.[59-61] It has been shown that in humans, the interneuronal network is expanded compared to rodents,[62] excitatory synaptic terminals onto FSINs have larger active zones with more functional release sites,[50] and a single AP from the presynaptic PN can produce large EPSPs at postsynaptic FSINs capable of driving APs[47,50,51,53,63] or even long-term plasticity.[51] Our findings demonstrate that both the intrinsic and synaptic excitability of human FSINs were reduced in FCD I epilepsy. Specifically, FSINs exhibited decreased firing rates, had increased single synaptic conductance from inhibitory inputs, and reduced connectivity from excitatory inputs. Consequently, excitatory synaptic conductance at FSINs was always smaller than the inhibitory conductance in FCD I epilepsy, departing from the E-I balance preserved in the non-epileptic cortex across species. Our results also suggest how intracortical electric stimulation protocols in clinical settings consisting of prolonged high-frequency, high-amplitude trains may be effective at temporarily restoring cortical E-I balance, if FSINs but not PNs were able to reliably translate direct local electric stimulation to AP output with high fidelity during such trains.

At the single synapse level, the higher inhibitory synaptic conductance at postsynaptic FSINs in FCD I epilepsy was accompanied by a larger increase from spontaneous inhibitory conductance. Despite involving different release machinery, spontaneous and evoked release are known to originate from the same vesicle pool.[64,65] Since G_{min} corresponds to synaptic release from AP-evoked Ca^{2+} influx whereas G_s includes release events from both AP firing and from stochastic opening of Ca^{2+} channels, G_{min}/G_s can thus be assumed to loosely represent

AP-induced enhancement of presynaptic release. We note again that G_s was calculated from spontaneous events, rather than miniature postsynaptic currents (mEPSC and mIPSC) measured in the presence of a sodium channel blocker that are more appropriate for isolating AP-independent release; nevertheless, the amplitudes and frequencies of miniature synaptic events were not noticeably different from spontaneous events albeit from a limited number of observations (Supplementary Fig. S10), and the firing rates of human neurons measured in vivo are very low,[66] such that the difference between spontaneous and miniature conductances on average can be assumed to be not substantial. In the control group, G_{min} was twice as large than G_s for excitatory inputs but equal for inhibitory inputs ($G_{E,min}/G_{E,s}$ = 2.0; $G_{I,min}/G_{I,s}$ = 1.0); on the other hand, G_{min} was larger than G_s for both excitatory and inhibitory inputs in FCD I epilepsy ($G_{E,min}/G_{E,s}$ = 2.7; $G_{I,min}/G_{I,s}$ = 2.1). We thus hypothesize that the AP broadening observed from FSINs in FCD I epilepsy may account for the increased single inhibitory synaptic conductance, considering that FSINs receive by far the most inhibitory input from other FSINs as their presynaptic partners,[42] and that $G_{I,min}/G_{I,s}$ was larger in FCD I epilepsy for both postsynaptic FSINs and PNs (1.0 vs. 2.1 at FSINs; 1.2 vs. 1.8 at PNs).

While both depolarization and repolarization were slower in FSINs in epilepsy, only the rate of repolarization was correlated with AP half-width, which in turn correlated with firing rate. Since the voltage-gated potassium channels (VGKC) are primarily responsible for repolarization following AP firing, finding the specific VGKC subtypes involved with the slower repolarization at FSINs in epilepsy is of much interest in therapeutic development. The K_v3 family, including the $K_v3.1$ subunit that is predominantly expressed in FSINs, is well known to be critically involved with the fast-spiking property of these interneurons. Novel potassium channel openers targeting the $K_v7.2$ and $K_v7.3$ subunits that had been previously implicated with epilepsy[67,68] are undergoing clinical trial for potential treatment of focal epilepsy,[69] and overexpression of potassium channels through gene therapy has been found to

produce antiepileptic effects in mouse models of FCD.[70] Given that the epileptogenic mechanisms may be distinct for different types of FCD, focusing on the VGKC subtype that may be specifically affected by a particular type of FCD could present an effective strategy for successful clinical translation.

Oscillatory activity, characterized by the synchronized firing of PN populations, is primarily generated by post-inhibition excitation.[71,72] pHFOs, which are markers of epileptic discharges, are regulated by PVINs that are involved with the generation, propagation, and termination of ictal activity.[73-78] Previous studies using mouse models showed that the propagation of ictal activity is opposed by PVIN-mediated inhibition.[79,80] Collectively, our data support the notion that synaptic changes at FSINs in FCD I epilepsy may contribute to the generation and propagation of epileptic discharges and pHFOs. This could involve increased synchrony of post-IPSP spikes, or a larger number of PNs synchronized simultaneously by each FSIN.[72,75,76,79,81] Since the number of FSINs is also decreased in FCD I,[20-22] epileptic discharges generated at the epileptic core may not be effectively suppressed, leading to their continuous generation.[75,79] While the present study focused on the superficial layers, further studies incorporating both superficial and deeper layers together with local field potential measurements would be instrumental in exploring the epileptogenic dynamics of the broader cortical network. Given that seizure is a dynamic rather than a static state, studies with induced seizure states through pharmacological or other manipulations would also provide useful in extending our findings to seizure susceptibility.

Regardless of our efforts to nominate the cellular substrates that are most relevant to pHFO generation and seizure propagation in vivo, the precise causal mechanisms responsible for these phenomena remain to be further clarified. As the main body of our data was obtained from ex vivo slice experiments, we are fundamentally limited to correlative analyses in comparing these two dissociated systems. Ideally, to address the causality of these clinical manifestations

adequately would accordingly require investigations using clinically oriented methodology encompassing treatment and effect observed from human patients. Within the present study and its boundaries, we do not claim to produce immediate answers to those questions; instead, we present these data as a resource that may assist future investigations, especially considering the scarcity of empirical evidence available to this date regarding the cellular physiology of human neurons obtained from unfixed human brain tissue.

Methods

Human brain slices

All protocols of this study were approved by the Seoul National University Hospital (SNUH) Institutional Review Board (IRB) (2012-194-1191). All human participants gave informed consent for tissue donation. Human brain tissue was obtained from patients with pharmaco-resistant epilepsy associated with focal cortical dysplasia type I (FCD I), and from patients with brain tumor, who underwent surgery at SNUH Department of Neurosurgery. 15 epilepsy patients and 10 tumor patients of ages 18-76, male and female, were included in this study (Supplementary Table 1). Patients in the epilepsy group were diagnosed with FCD I or III (FCD I accompanied by heterogenous lesions) by pathological examinations following surgery. Cortical tissue originated from the temporal (n = 13), frontal (n = 9), parietal (n = 2), and occipital (n = 1) area. Tissue from epilepsy patients were obtained from the ictal onset zone. Tissue from tumor patients were obtained from a non-pathological region resected in the course of approaching the tumor during surgery. No analysis based on patient sex was performed due to the limited sample size after grouping with both diagnosis and sex. No participant compensation was made.

After en bloc surgical resection, tissue was immediately placed in an ice-cold solution at the operating theater. The solution used for transport and slicing contained (in mM): 110 choline chloride, 26 $NaHCO_3$, 2.5 KCl, 3.1 Na-pyruvate, 11.6 Na-ascorbate, 1.25 NaH_2PO_4, 10 D-glucose, 0.5 $CaCl_2$, 7 $MgCl_2$, pH adjusted to 7.4, 300-310 mOsm. The tissue container was kept in a thermally isolated transportation box filled with ice and transported from the operating room at SNUH to the laboratory at Seoul National University (SNU) College of Medicine within 20 minutes. The tissue block was then placed orthogonal to the pia to preserve cortical

layers and white matter in proper orientation. Slices of 300 μm thickness were prepared with a vibratome (VT1200S, Leica), and allowed to recover at 36 ℃ for 10 minutes before being maintained at room temperature for an additional 1 hour in artificial cerebrospinal fluid (aCSF) containing (in mM): 124 NaCl, 26 $NaHCO_3$, 2.5 KCl, 1.25 NaH_2PO_4, 10 D-glucose, 2.5 $CaCl_2$, 1.3 $MgCl_2$, pH adjusted to 7.4, 300-310 mOsm. The same aCSF was used for recordings. All solutions were continuously aerated with carbogen (95% O_2 / 5% CO_2) throughout the course of experiments, including transport and slicing. Experiments were performed within a 24-hour period after slicing.

Rodent brain slices

All experimental protocols were approved by the SNU Institutional Animal Care and Use Committee (IACUC) (SNU-201119-5-1). A total of 30 male and female Sprague-Dawley rats (*Rattus norvegicus*), ages 4 to 5 weeks, were used for this study. Animals were housed under standard environmental conditions (24-hour light/dark cycle) in a temperature-and-humidity-controlled room (25 ± 2 ℃) and were given food and water ad libitum, with veterinary supervision from SNU College of Medicine Institute for Experimental Animals. Animals were anesthetized by inhalation of 5% (v/v) isoflurane and rapidly decapitated, after which the whole brain was removed and placed onto the vibratome. Rat brain slices containing the temporal association area (TeA) were prepared with identical solutions to those used for human brain slices.

ex vivo electrophysiology

All human and rat experiments were conducted under identical conditions. Slices were immersed in a recording chamber and perfused with the recording aCSF (30 ± 2 °C) using a peristaltic pump (2-4 mL/min). All recordings were made from the soma of fast-spiking interneurons (FSINs) or pyramidal neurons (PNs) in layer 2/3 (L2/3) of the neocortex. Patch pipettes (3-7 MΩ) and monopolar stimulation pipettes (1-2 MΩ) were pulled from borosilicate glass capillaries using a PC-10 pipette puller (Narishige). Patch pipettes were filled with internal solution containing (in mM): 130 K-gluconate, 7 KCl, 2 NaCl, 1 $MgCl_2$, 0.1 EGTA, 2 Mg-ATP, 0.3 Na_2-GTP, 10 HEPES, and 0.2% (w/v) biocytin, adjusted to pH 7.3 with KOH, and 295-300 mOsm with sucrose. Cells with series resistance (R_s) below 25 MΩ were accepted, and R_s was fully monitored and compensated throughout the course of recordings. 100 µM D-2-amino-5-phosphonopentanoic acid (D-APV, Tocris) was bath-applied to prevent potential long-term plasticity caused by continued stimulation. Data were acquired using a MultiClamp 700B amplifier with Digidata 1440A digitizer and pClamp 10 (Molecular Devices) or an EPC-10 amplifier and Patchmaster 2x90 (HEKA), at a sampling rate of 10 kHz.

Cells were held in current clamp at 0 pA to measure the following parameters, 5 minutes after break-in: (1) resting membrane potential (RMP), (2) input resistance (R_{in}), (3) sag ratio, (4) firing frequency in response to somatic current injection (f-i), (5) derivative of membrane potential with respect to time (dV/dt), (6) action potential (AP) threshold, and (7) AP half-width. R_{in} and sag ratio were calculated from membrane potential responses to a hyperpolarizing current input (-50 pA, 500 ms). Likewise, step current injections of 500 ms duration with amplitudes up to 500 pA in 50 pA increments were applied to obtain the f-i curve. The resulting firing patterns were used to identify the cell type. The first AP generated at rheobase was used to analyze the dV/dt, AP threshold, and AP half-width. AP threshold was defined as the membrane potential at which dV/dt first exceeded 10 (V/s). AP amplitude was

calculated as the difference between the AP peak and the AP threshold, and the width at half of this amplitude was taken as AP half-width. Liquid junction potential was not corrected for in the membrane potential values reported in this study, but taken into account in calculating synaptic conductances from measured postsynaptic current amplitudes (see below).

Spontaneous and evoked postsynaptic currents were recorded under voltage clamp. Cells were first held at -70 mV for excitatory inputs, then at 0 mV for inhibitory inputs. Excitatory and inhibitory synaptic conductances (G_E and G_I, respectively) were calculated from postsynaptic current amplitudes, using their respective reversal potentials (E_{rev}) for nonselective cationic conductance through AMPA receptors at 0 mV or Cl^- conductance through $GABA_A$ receptors at -65 mV, and liquid junction potential of approximately 15 mV obtained from our experimental conditions. Spontaneous excitatory postsynaptic currents (sEPSC) were recorded for at least 1 minute, and spontaneous inhibitory postsynaptic currents (sIPSC) were recorded for at least 5 minutes, from each cell. Evoked excitatory and inhibitory postsynaptic currents (eEPSC and eIPSC, respectively) were similarly recorded from the same cells. For extracellular stimulation, monopolar glass stimulation electrodes filled with aCSF were positioned within L2/3, typically 50 to 150 μm away from the somata of recorded cells. Stimuli were delivered via an isolator (DLS100, WPI) controlled by a waveform generator (DS8000, WPI). For minimal stimulation, we took the stimulation intensity at which eEPSC was produced with a synaptic failure rate of approximately 50%. Under our conditions, minimal stimulation intensity was typically between 2 to 6 V for both FSINs and PNs, which was not significantly different between control and epilepsy groups for both FSINs (control, 4.2 ± 0.4 V; epilepsy, 4.6 ± 0.4 V) and PNs (control, 3.9 ± 0.3 V; epilepsy, 4.3 ± 0.3 V), or between FSINs and PNs from the same group. G_{max}/G_{min} below 1 were rounded up to 1. Stimulation site was selected such that large eEPSC could be reliably produced in response to broad-scale synaptic activation at a higher stimulation intensity (referred to as maximal stimulation; see Results), and was

unchanged between minimal and maximal stimulation. Both eEPSC and eIPSC were evoked using the same stimulation intensity and electrode position for each cell.

Histology and imaging

Neurons were filled with the internal solution containing 0.2% (w/v) biocytin for at least 15 minutes during electrophysiological recordings. At the end of all experiments, slices were fixed in 4% (v/v) paraformaldehyde (PFA) in phosphate-buffered saline (PBS) for less than 24 hours at 4 °C, rinsed three times with PBS, followed by subsequent immunocytochemical staining procedures. Slices were incubated in permeabilization buffer (0.3% (v/v) Triton X-100, Sigma-Aldrich) for 30 minutes (10 minutes, refreshed three times) then transferred to blocking buffer (0.3% (v/v) Triton X-100, 0.5% (w/v) Bovine Serum Albumin (BSA, Bovagen)) and kept at room temperature for a total of 3 hours (1 hour, refreshed three times). Slices were conjugated with streptavidin-Cy3 (1:500, Invitrogen) overnight at 4 °C, triple-washed with PBS, and mounted on glass coverslips with a medium containing 4',6-diamidino-2-phenylindole (DAPI, Abcam). Slices were imaged using a laser scanning confocal microscope (Leica) and analyzed with LAS X (Leica) and ImageJ (NIH). Dendritic and somatic morphology of cells were used for post hoc confirmation of the cell type in addition to prior electrophysiological characterization. Cells with somata located within the cortical depth of 1200 μm from pia were taken as L2/3 neurons.[35,54,82]

Intracranial electroencephalography

Intracranial electroencephalography (iEEG) data were collected from patients with medically intractable epilepsy implanted with subdural electrode grids and depth electrodes, diagnosed

with FCD I by pathology (Supplementary Table 1). Conventional and/or high-density subdural electrodes (contact diameter, 3 or 2 mm; inter-electrode distance, 10 or 5 mm, respectively; Ad-tech Medical Instrument and PMT) as well as depth electrodes (contact diameter, 5 mm; inter-electrode distance, 10 mm; PMT) were implanted as clinically needed. The precise positioning of the electrodes for each patient were determined using the CURRY software (Compumedics Neuroscan) through co-registration of preoperative magnetic resonance (MR) images and postoperative computed tomography (CT) images (Supplementary Fig. S9).

Signals were recorded by a 128-channel amplifier system (Neuvo EEG; Compumedics Neuroscan) at a sampling rate of 2 kHz. Cortical areas corresponding to the ictal onset zone and those exhibiting high-frequency oscillations (HFOs) were identified separately. The ictal onset zone was defined as the region that initially displayed seizure activity. Pathological high-frequency oscillations (pHFOs) were identified by their characteristic high frequency and association with spikes or pathological slowing via visual inspection during both interictal and ictal phases.[28,83] We excluded putative physiological HFOs, especially ripples at the frequency range of 80 to 200 Hz, which are typically not associated with spikes or pathological slowing and mainly observed in the auditory, visual, and somatosensory areas.[26] Clinical evaluations were conducted by epileptologists at SNUH Department of Neurology.

From a 24-hour monitoring period, data from a one-hour segment between 9 to 11 AM were selected for pHFO detection during a stable, awake resting state. Signals were notch-filtered to remove line noise at 60 Hz and its related harmonics. Given that pHFOs are defined as ripples (80-200 Hz) and fast ripples (200-500 Hz),[30,84] signals were band-pass filtered for this frequency range using a 4^{th}-order Butterworth filter. The short-time energy (STE) method was used to automatically detect HFOs from preprocessed signals.[85] STE from signal x(t) was defined by:

$$\mathrm{STE(t)} = \sqrt{\frac{1}{\mathrm{N}} \sum_{i=t-N+1}^{t} x(i)^2}$$

where N represents a window size of 3 ms. To correct against capacitive artifacts, we applied a winsorization strategy by replacing STE values exceeding 10 standard deviations (SD) above the median, by median + 10 SD. pHFOs were then detected using RIPPLELAB.[82,84,86] Specifically, the winsorized data were segmented into 10-minute epochs, after which the median and SD of STEs within each epoch were recalculated. We defined windows as those representing pHFOs when two or more consecutive windows were associated with STE values above median + 5 SD, and accompanied by more than 6 peaks per window with amplitudes larger than mean + 3 SD of the rectified band-pass filtered signal. Multiple windows meeting these criteria which were separated by less than 10 ms were taken together to be corresponding to a single pHFO event.[86,87]

Statistics and reproducibility

Data from human patients were collected as available according to the surgical schedule. For human samples, no statistical method was used to predetermine sample size. No data that met the quality standards for electrophysiological recordings as described earlier were excluded from the analyses. Cells were chosen randomly from L2/3 of the neocortex for ex vivo electrophysiology recordings. The investigators were not blinded to allocation during experiments and outcome assessment. Statistical tests were performed using two-sided Mann-Whitney U test or two-sided unpaired t-test where applicable, as stated in the figure legends. For correlative analyses between variables representing ex vivo data, the Pearson correlation coefficient was used to determine the goodness of fit for linear regressions as well as its

significance, since not only the ranks but also the quantities of these variables are meaningful and sample sizes were sufficiently large. F-tests were used to determine the deviation from zero of the slopes of linear regressions. For correlative analyses between ex vivo and in vivo data, the Spearman correlation coefficient was additionally used for robustness as the number of samples in these cases was limited by the number of human patients diagnosed with FCD I epilepsy, with iEEG recordings that exhibited pHFOs during resting state, hence affecting the assumption of normality relevant to the Pearson coefficient. Statistical information is expressed as mean ± standard error of the mean (SEM), with n indicating the number of cells. Error bars indicate SEM. Statistical significance was accepted when $P < 0.05$ (* $P < 0.05$; ** $P < 0.01$; *** $P < 0.001$). Correlations were considered positive when each coefficient was greater than +0.2, or negative when it was smaller than -0.2, with associated $P < 0.05$.

Data analysis

Data were analyzed and visualized using custom codes written in MATLAB (MathWorks) including PVBS (https://github.com/flosfor/pvbs), RIPPLELAB (https://github.com/BSP-Uniandes/RIPPLELAB), in addition to other software including ClampFit 11 (Molecular Devices), Igor Pro 7 (Wavemetrics), and Prism 8 (GraphPad).

Data availability

The data that support the findings of this study are available from the corresponding authors upon request. Source data are provided with this paper.

Code availability

Custom codes used for the present study in addition to other software as described in the Methods are available from the following sources: PVBS (https://github.com/flosfor/pvbs), RIPPLELAB (https://github.com/BSP-Uniandes/RIPPLELAB).

References

1. Engel, J. Excitation and inhibition in epilepsy. *Canadian Journal of Neurological Sciences* 23, 167-174 (1996).

2. Dehghani, N.*, et al.* Dynamic balance of excitation and inhibition in human and monkey neocortex. *Scientific reports* 6, 1-12 (2016).

3. Chen, Z., Brodie, M.J., Liew, D. & Kwan, P. Treatment outcomes in patients with newly diagnosed epilepsy treated with established and new antiepileptic drugs: a 30-year longitudinal cohort study. *JAMA neurology* 75, 279-286 (2018).

4. Kwan, P., Schachter, S.C. & Brodie, M.J. Drug-resistant epilepsy. *New England Journal of Medicine* 365, 919-926 (2011).

5. Sisodiya, S. Surgery for focal cortical dysplasia. *Brain* 127, 2383-2384 (2004).

6. Tassi, L.*, et al.* Type I focal cortical dysplasia: surgical outcome is related to histopathology. *Epileptic Disorders* 12, 181-191 (2010).

7. Blümcke, I.*, et al.* The clinicopathologic spectrum of focal cortical dysplasias: A consensus classification proposed by an ad hoc task force of the ILAE Diagnostic Methods Commission 1. (Wiley Online Library, 2011).

8. Marcelis, S., Bossche, S.V. & Dekeyzer, S. Not Your Everyday FCD: Imaging Findings of Focal Cortical Dysplasia Type 1. *Journal of the Belgian Society of Radiology* 106 (2022).

9. Takei, N. & Nawa, H. mTOR signaling and its roles in normal and abnormal brain development. *Frontiers in Molecular Neuroscience* 7 (2014).

10. Ryskalin, L.*, et al.* mTOR-Dependent Cell Proliferation in the Brain. *BioMed Research International* 2017, 7082696 (2017).

11. Iffland, P.H. & Crino, P.B. Focal cortical dysplasia: gene mutations, cell signaling, and therapeutic implications. *Annual Review of Pathology: Mechanisms of Disease* 12, 547-571 (2017).

12. Jesus-Ribeiro, J.*, et al.* Genomic and epigenetic advances in focal cortical dysplasia types I and II: A scoping review. *Frontiers in neuroscience*, 1412 (2021).

13. Chung, C.K., Lee, S.K. & Kim, K.J. Surgical outcome of epilepsy caused by cortical dysplasia. *Epilepsia* 46, 25-29 (2005).

14. Lamberink, H., Otte, W., Blumcke, I. & Braun, K. Seizure outcome and drug-freedom related to histopathology up to 5 years after epilepsy surgery: a retrospective, multi-centre, longitudinal, cohort study. *Lancet Neurol* 19, 748-757 (2020).

15. Shu, Y., Hasenstaub, A. & McCormick, D.A. Turning on and off recurrent balanced cortical activity. *Nature* 423, 288-293 (2003).

16. Haider, B., Duque, A., Hasenstaub, A.R. & McCormick, D.A. Neocortical network activity in vivo is generated through a dynamic balance of excitation and inhibition. *Journal of Neuroscience* 26, 4535-4545 (2006).

17. Calcagnotto, M.E., Paredes, M.F., Tihan, T., Barbaro, N.M. & Baraban, S.C. Dysfunction of synaptic inhibition in epilepsy associated with focal cortical dysplasia. *Journal of Neuroscience* 25, 9649-9657 (2005).

18. Banerjee, J.*, et al.* GABAA receptor-mediated epileptogenicity in focal cortical dysplasia (FCD) depends on age at epilepsy onset. *Frontiers in cellular neuroscience* 14, 562811 (2020).

19. Cheng, L.*, et al.* Mechanistic Analysis of Micro-Neurocircuits Underlying the Epileptogenic Zone in Focal Cortical Dysplasia Patients. *Cerebral Cortex* 32, 2216-2230 (2022).

20. Rosen, G., Jacobs, K. & Prince, D. Effects of neonatal freeze lesions on expression of parvalbumin in rat neocortex. *Cerebral cortex (New York, NY: 1991)* 8, 753-761 (1998).

21. Roper, S.N., Eisenschenk, S. & King, M.A. Reduced density of parvalbumin-and calbindin D28k-immunoreactive neurons in experimental cortical dysplasia. *Epilepsy research* 37, 63-71 (1999).

22. Medici, V.*, et al.* Different parvalbumin and GABA expression in human epileptogenic focal cortical dysplasia. *Epilepsia* 57, 1109-1119 (2016).

23. Brooks-Kayal, A.R., Shumate, M.D., Jin, H., Rikhter, T.Y. & Coulter, D.A. Selective changes in single cell GABAA receptor subunit expression and function in temporal lobe epilepsy. *Nature medicine* 4, 1166-1172 (1998).

24. Bragin, A., Engel Jr, J., Wilson, C.L., Fried, I. & Mathern, G.W. Hippocampal and entorhinal cortex high-frequency oscillations (100–500 Hz) in human epileptic brain and in kainic acid-treated rats with chronic seizures. *Epilepsia* 40, 127-137 (1999).

25. Pail, M.*, et al.* High frequency oscillations in epileptic and non-epileptic human hippocampus during a cognitive task. *Scientific reports* 10, 18147 (2020).

26. Thomschewski, A., Hincapié, A.-S. & Frauscher, B. Localization of the epileptogenic zone using high frequency oscillations. *Frontiers in neurology* 10, 94 (2019).

27. Jacobs, J.*, et al.* High-frequency electroencephalographic oscillations correlate with outcome of epilepsy surgery. *Annals of Neurology: Official Journal of the American Neurological Association and the Child Neurology Society* 67, 209-220 (2010).

28. Frauscher, B.*, et al.* High-frequency oscillations: the state of clinical research. *Epilepsia* 58, 1316-1329 (2017).

29. Hussain, S.A.*, et al.* Intraoperative fast ripples independently predict postsurgical epilepsy outcome: comparison with other electrocorticographic phenomena. *Epilepsy research* 135, 79-86 (2017).

679 30. Jiruska, P.*, et al.* Update on the mechanisms and roles of high-frequency oscillations in
680 seizures and epileptic disorders. *Epilepsia* 58, 1330-1339 (2017).
681 31. Jefferys, J.G.*, et al.* Mechanisms of physiological and epileptic HFO generation.
682 *Progress in neurobiology* 98, 250-264 (2012).
683 32. Fink, C.G., Gliske, S., Catoni, N. & Stacey, W.C. Network mechanisms generating
684 abnormal and normal hippocampal high-frequency oscillations: a computational analysis.
685 *Eneuro* 2 (2015).
686 33. Du, F.*, et al.* Preferential neuronal loss in layer III of the entorhinal cortex in patients
687 with temporal lobe epilepsy. *Epilepsy research* 16, 223-233 (1993).
688 34. Hadjivassiliou, G.*, et al.* The application of cortical layer markers in the evaluation of
689 cortical dysplasias in epilepsy. *Acta neuropathologica* 120, 517-528 (2010).
690 35. Kalmbach, B.E.*, et al.* h-Channels contribute to divergent intrinsic membrane
691 properties of supragranular pyramidal neurons in human versus mouse cerebral cortex. *Neuron*
692 100, 1194-1208. e1195 (2018).
693 36. Nunez, P.L. & Srinivasan, R. *Electric fields of the brain: the neurophysics of EEG*
694 (Oxford University Press, USA, 2006).
695 37. Lindén, H.*, et al.* LFPy: a tool for biophysical simulation of extracellular potentials
696 generated by detailed model neurons. *Frontiers in neuroinformatics* 7, 41 (2014).
697 38. Anastassiou, C.A., Perin, R., Markram, H. & Koch, C. Ephaptic coupling of cortical
698 neurons. *Nature neuroscience* 14, 217-223 (2011).
699 39. Campagnola, L.*, et al.* Local connectivity and synaptic dynamics in mouse and human
700 neocortex. *Science* 375, eabj5861 (2022).
701 40. Tsodyks, M.V., Skaggs, W.E., Sejnowski, T.J. & McNaughton, B.L. Paradoxical
702 effects of external modulation of inhibitory interneurons. *Journal of neuroscience* 17, 4382-
703 4388 (1997).

704 41. Hansel, D., & Mato, G. Short-term plasticity explains irregular persistent activity in
705 working memory tasks. *Journal of Neuroscience* 33(1), 133-149 (2013).
706 42. Pfeffer, C. K., Xue, M., He, M., Huang, Z. J., & Scanziani, M. Inhibition of inhibition
707 in visual cortex: the logic of connections between molecularly distinct interneurons. *Nature*
708 *neuroscience* 16(8), 1068-1076 (2013).
709 43. Baraban, S.C. Epileptogenesis in the dysplastic brain: a revival of familiar themes.
710 *Epilepsy Currents* 1, 6-11 (2001).
711 44. Marin-Valencia, I., Guerrini, R. & Gleeson, J.G. Pathogenetic mechanisms of focal
712 cortical dysplasia. *Epilepsia* 55, 970-978 (2014).
713 45. Koh, H.Y.*, et al.* Non–cell autonomous epileptogenesis in focal cortical dysplasia.
714 *Annals of Neurology* 90, 285-299 (2021).
715 46. Janca, R.*, et al.* Distinct patterns of interictal intracranial EEG in focal cortical dysplasia
716 type I and II. *Clinical Neurophysiology* 151, 10-17 (2023).
717 47. Molnár, G.*, et al.* Complex events initiated by individual spikes in the human cerebral
718 cortex. *PLoS biology* 6, e222 (2008).
719 48. Verhoog, M.B.*, et al.* Mechanisms underlying the rules for associative plasticity at adult
720 human neocortical synapses. *Journal of Neuroscience* 33, 17197-17208 (2013).
721 49. Verhoog, M.B.*, et al.* Layer-specific cholinergic control of human and mouse cortical
722 synaptic plasticity. *Nature communications* 7, 12826 (2016).
723 50. Molnár, G.*, et al.* Human pyramidal to interneuron synapses are mediated by multi-
724 vesicular release and multiple docked vesicles. *Elife* 5, e18167 (2016).
725 51. Szegedi, V.*, et al.* Plasticity in single axon glutamatergic connection to GABAergic
726 interneurons regulates complex events in the human neocortex. *PLoS biology* 14, e2000237
727 (2016).

52. Testa-Silva, G.*, et al.* High synaptic threshold for dendritic nmda spike generation in human layer 2/3 pyramidal neurons. *Cell reports* 41 (2022).

53. Hunt, S.*, et al.* Strong and reliable synaptic communication between pyramidal neurons in adult human cerebral cortex. *Cerebral Cortex* 33, 2857-2878 (2023).

54. Yoon, J. Geometrical determinant of nonlinear synaptic integration in human cortical pyramidal neurons. *bioRxiv* (2024). DOI: 10.1101/2024.07.14.601255

55. Hutsler, J.J., Lee, D.-G. & Porter, K.K. Comparative analysis of cortical layering and supragranular layer enlargement in rodent carnivore and primate species. *Brain research* 1052, 71-81 (2005).

56. Goulas, A., Zilles, K. & Hilgetag, C.C. Cortical gradients and laminar projections in mammals. *Trends in Neurosciences* 41, 775-788 (2018).

57. Galakhova, A.*, et al.* Evolution of cortical neurons supporting human cognition. *Trends in Cognitive Sciences* 26, 909-922 (2022).

58. Markov, N. T., Ercsey-Ravasz, M., Van Essen, D. C., Knoblauch, K., Toroczkai, Z., & Kennedy, H. Cortical high-density counterstream architectures. *Science* 342(6158), 1238406 (2013).

59. Jiang, X., Lachance, M. & Rossignol, E. Involvement of cortical fast-spiking parvalbumin-positive basket cells in epilepsy. *Progress in Brain Research* 226, 81-126 (2016).

60. Marín, O. Interneuron dysfunction in psychiatric disorders. *Nature Reviews Neuroscience* 13, 107-120 (2012).

61. Staley, K. Molecular mechanisms of epilepsy. *Nature neuroscience* 18, 367-372 (2015).

62. Loomba, S.*, et al.* Connectomic comparison of mouse and human cortex. *Science* 377, eabo0924 (2022).

752 63. Szegedi, V.*, et al.* High-precision fast-spiking basket cell discharges during complex
753 events in the human neocortex. *Eneuro* 4 (2017).
754 64. Groemer, T.W. & Klingauf, J. Synaptic vesicles recycling spontaneously and during
755 activity belong to the same vesicle pool. *Nature neuroscience* 10, 145-147 (2007).
756 65. Hua, Y., Sinha, R., Martineau, M., Kahms, M. & Klingauf, J. A common origin of
757 synaptic vesicles undergoing evoked and spontaneous fusion. *Nature neuroscience* 13, 1451-
758 1453 (2010).
759 66. Chung, J. E., *et al*. (2022). High-density single-unit human cortical recordings using
760 the Neuropixels probe. Neuron, 110(15), 2409-2421.
761 67. Miceli, F.*, et al.* The voltage-sensing domain of Kv7. 2 channels as a molecular target
762 for epilepsy-causing mutations and anticonvulsants. *Frontiers in pharmacology* 2, 2 (2011).
763 68. Miceli, F.*, et al.* Early-onset epileptic encephalopathy caused by gain-of-function
764 mutations in the voltage sensor of Kv7. 2 and Kv7. 3 potassium channel subunits. *Journal of*
765 *Neuroscience* 35, 3782-3793 (2015).
766 69. French, J.A.*, et al.* Efficacy and Safety of XEN1101, a Novel Potassium Channel
767 Opener, in Adults With Focal Epilepsy: A Phase 2b Randomized Clinical Trial. *JAMA*
768 *neurology* (2023).
769 70. Kiani, L. Gene therapy for seizures in focal cortical dysplasia. *Nature Reviews*
770 *Neurology* 1-1 (2024).
771 71. Mann, E.O. & Paulsen, O. Role of GABAergic inhibition in hippocampal network
772 oscillations. *Trends in neurosciences* 30, 343-349 (2007).
773 72. Cobb, S., Buhl, E.H., Halasy, K., Paulsen, O. & Somogyi, P. Synchronization of
774 neuronal activity in hippocampus by individual GABAergic interneurons. *Nature* 378, 75-78
775 (1995).

776 73. Bartos, M., Vida, I. & Jonas, P. Synaptic mechanisms of synchronized gamma
777 oscillations in inhibitory interneuron networks. *Nature reviews neuroscience* 8, 45-56 (2007).
778 74. Kuki, T.*, et al.* Contribution of parvalbumin and somatostatin-expressing GABAergic
779 neurons to slow oscillations and the balance in beta-gamma oscillations across cortical layers.
780 *Frontiers in neural circuits* 9, 6 (2015).
781 75. Klausberger, T.*, et al.* Brain-state-and cell-type-specific firing of hippocampal
782 interneurons in vivo. *Nature* 421, 844-848 (2003).
783 76. Klausberger, T.*, et al.* Complementary roles of cholecystokinin-and parvalbumin-
784 expressing GABAergic neurons in hippocampal network oscillations. *Journal of Neuroscience*
785 25, 9782-9793 (2005).
786 77. Benarroch, E.E. Neocortical interneurons: functional diversity and clinical correlations.
787 *Neurology* 81, 273-280 (2013).
788 78. Gulyás, A.I. & Freund, T.T. Generation of physiological and pathological high
789 frequency oscillations: the role of perisomatic inhibition in sharp-wave ripple and interictal
790 spike generation. *Current opinion in neurobiology* 31, 26-32 (2015).
791 79. Sessolo, M.*, et al.* Parvalbumin-positive inhibitory interneurons oppose propagation but
792 favor generation of focal epileptiform activity. *Journal of Neuroscience* 35, 9544-9557 (2015).
793 80. Cammarota, M., Losi, G., Chiavegato, A., Zonta, M. & Carmignoto, G. Fast spiking
794 interneuron control of seizure propagation in a cortical slice model of focal epilepsy. *The*
795 *Journal of Physiology* 591, 807-822 (2013).
796 81. de Curtis, M. & Avoli, M. GABAergic networks jump-start focal seizures. *Epilepsia*
797 57, 679-687 (2016).
798 82. Mohan, H.*, et al.* Dendritic and axonal architecture of individual pyramidal neurons
799 across layers of adult human neocortex. *Cerebral Cortex* 25, 4839-4853 (2015).

800 83. Sato, Y., *et al.* Preictal surrender of post–spike slow waves to spike-related high-
801 frequency oscillations (80–200 Hz) is associated with seizure initiation. *Epilepsia* 55, 1399-
802 1405 (2014).
803 84. de la Prida, L.M., Staba, R.J. & Dian, J.A. Conundrums of high-frequency oscillations
804 (80-800 Hz) in the epileptic brain. *Journal of clinical neurophysiology: official publication of*
805 *the American Electroencephalographic Society* 32, 207 (2015).
806 85. Staba, R.J., Wilson, C.L., Bragin, A., Fried, I. & Engel Jr, J. Quantitative analysis of
807 high-frequency oscillations (80–500 Hz) recorded in human epileptic hippocampus and
808 entorhinal cortex. *Journal of neurophysiology* 88, 1743-1752 (2002).
809 86. Navarrete, M., Alvarado-Rojas, C., Le Van Quyen, M. & Valderrama, M.
810 RIPPLELAB: A comprehensive application for the detection, analysis and classification of
811 high frequency oscillations in electroencephalographic signals. *PloS one* 11, e0158276 (2016).
812 87. Gardner, A.B., Worrell, G.A., Marsh, E., Dlugos, D. & Litt, B. Human and automated
813 detection of high-frequency oscillations in clinical intracranial EEG recordings. *Clinical*
814 *neurophysiology* 118, 1134-1143 (2007).

815

Author contributions

Conceptualization, E.C., C.K.C., J.Y., W.-K.H.; Investigation, E.C., J.K., G.L., J.S., J.Y.; Validation, E.C., H.L., S.-H.L., C.K.C., J.Y., W.-K.H.; Visualization, E.C., J.K., G.L., J.Y.; Resources, E.C., S.-H.L., C.K.C., J.Y., W.-K.H.; Writing - original draft, E.C., J.Y., W.-K.H.; Writing - review & editing, E.C., C.K.C., J.Y., W.-K.H.; Supervision, C.K.C., J.Y., W.-K.H.; Funding acquisition, S.-H.L., C.K.C., W.-K.H.

Acknowledgements

We thank Dr. Chul-Kee Park for providing human brain tissue obtained from tumor surgery, and Dr. Changhyeon Ryu for helpful comments on the manuscript. This study was supported by the National Research Foundation grants from the Republic of Korea Ministry of Science and ICT (2020R1A2B5B02002070 to W.-K.H. and 2021M3E5D9021887 to S.-H.L.), and the Alchemist Project (Fully implantable closed loop brain to X for voice communication) by the Ministry of Trade, Industry and Energy (20012355, NTIS 1415181023 to C.K.C.).

Competing interests

The authors report no competing interests.

836

837 Figures and legends

838

Figure 1

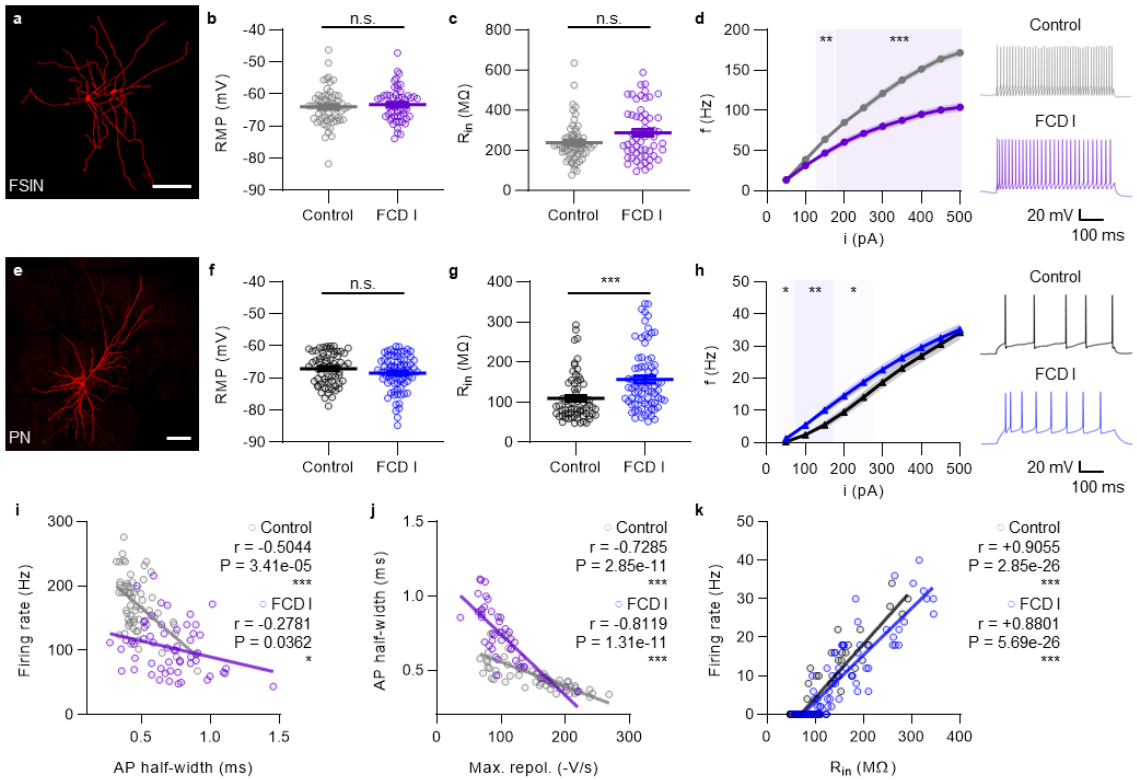
a
FSIN
b
n.s.
RMP (mV)
Control
FCD I
c
n.s.
R_{in} (MΩ)
d
**
***
f (Hz)
i (pA)
Control
FCD I
20 mV
100 ms
e
PN
f
g
***
h
*
i
Firing rate (Hz)
Control
r = -0.5044
P = 3.41e-05
FCD I
r = -0.2781
P = 0.0362
AP half-width (ms)
j
AP half-width (ms)
r = -0.7285
P = 2.85e-11
r = -0.8119
P = 1.31e-11
Max. repol. (-V/s)
k
r = +0.9055
P = 2.85e-26
r = +0.8801
P = 5.69e-26
R_{in} (MΩ)

Figure 1. Intrinsic membrane properties of human neocortical layer 2/3 (L2/3) fast-spiking interneurons (FSINs) and pyramidal neurons (PNs). (a) Representative FSINs. Scale bar, 100 μm. **(b)** Resting membrane potential (RMP). Control (gray), -64.0 ± 0.7 (mV) (n = 61); FCD I (purple), -63.2 ± 0.7 (mV) (n = 57); P = 0.4237. **(c)** Input resistance (R_{in}). Control, 237.4 ± 12.6 (MΩ) (n = 61); FCD I, 287.0 ± 17.1 (MΩ) (n = 57); P = 0.0578. **(d)** FSIN firing rate was lower in FCD I epilepsy. Control, n = 61; FCD I, n = 57. Representative traces are from +200 pA. **(e)** Representative PN. Scale bar, 100 μm. **(f)** RMP. Control (black), -67.1 ± 0.6 (mV) (n = 68); FCD I (blue), -68.4 ± 0.6 (mV) (n = 77); P = 0.1992. **(g)** PN R_{in} was higher in FCD I epilepsy. Control, 109.4 ± 7.0 (MΩ) (n = 68); FCD I, 156.7 ± 8.7 (MΩ) (n = 77); P = 1.21e-05. **(h)** PN firing rate was higher in FCD I epilepsy for smaller current inputs, but saturated towards similar maxima. Control, n = 68; FCD I, n = 77. Representative traces are from +200 pA. **(i)** FSIN maximum firing rate was negatively correlated with AP half-width (control, r = -0.5044, P = 3.41e-05; FCD I, r = -0.2781, P = 0.0362). **(j)** FSIN AP half-width was negatively correlated with the maximum rate of repolarization (control, r = -0.7285, P = 2.85e-11; FCD I, r = -0.8119, P = 1.31e-11). **(k)** PN firing rate at intermediate (+150 pA) current inputs was positively correlated with R_{in}. Control (r = +0.9055, P = 2.85e-26); FCD I (r = +0.8801, P = 5.69e-26). Throughout all figures, lines represent the mean and the standard error of the mean (SEM), and two-sided Mann-Whitney U tests were used for comparisons, unless otherwise specified. Statistical significance was accepted when $P < 0.05$ (* $P < 0.05$; ** $P < 0.01$; *** $P < 0.001$). Source data are provided with this paper.

Figure 2

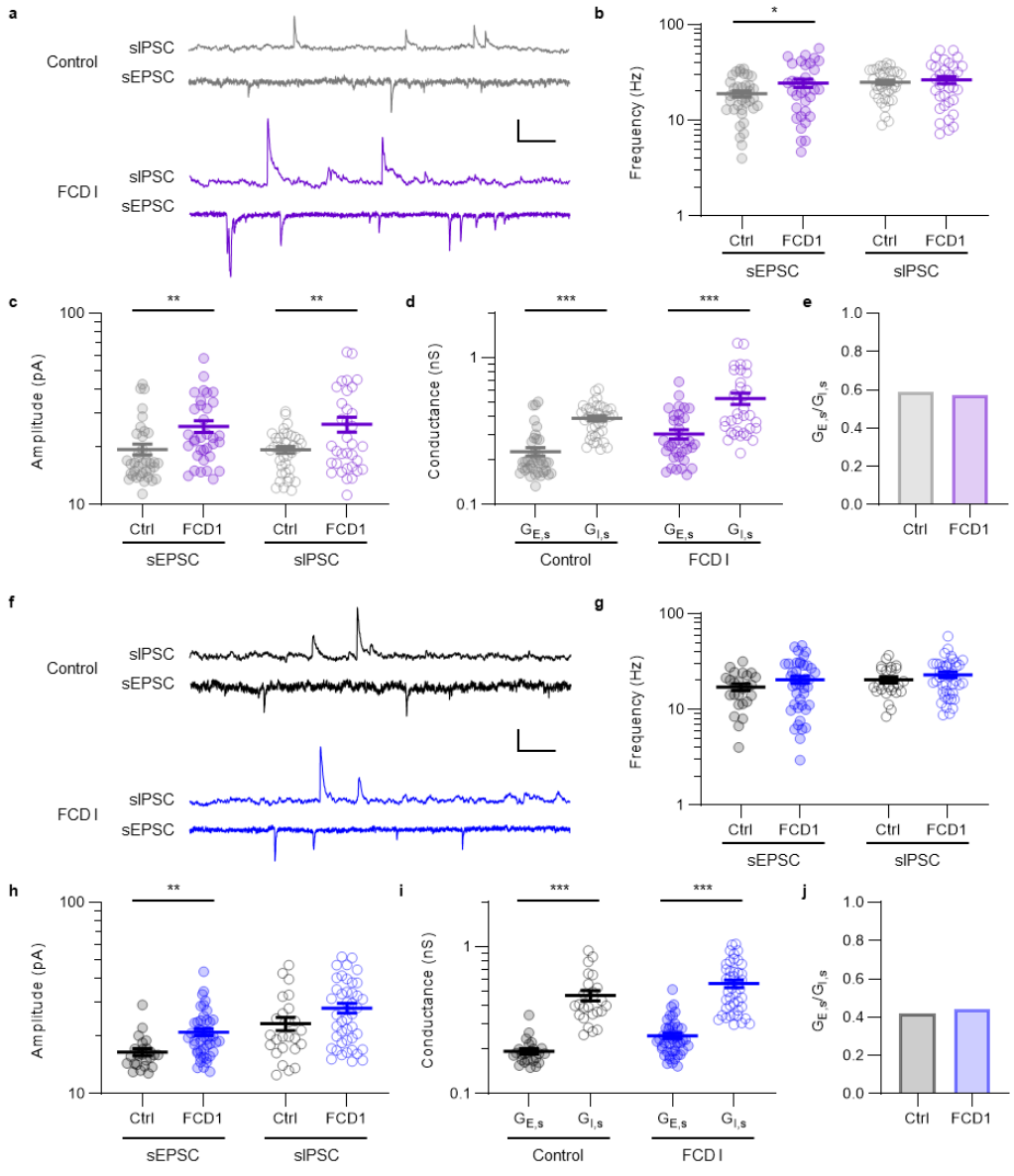
a
Control
sIPSC
sEPSC
FCD I
sIPSC
sEPSC
b
Frequency (Hz)
100
10
1
*
Ctrl
FCD1
Ctrl
FCD1
sEPSC
sIPSC
c
Amplitude (pA)
100
10
**
**
Ctrl
FCD1
Ctrl
FCD1
sEPSC
sIPSC
d
Conductance (nS)
1
0.1
***
***
G_E,s
G_I,s
G_E,s
G_I,s
Control
FCD I
e
G_E,s/G_I,s
1.0
0.8
0.6
0.4
0.2
0.0
Ctrl
FCD1
f
Control
sIPSC
sEPSC
FCD I
sIPSC
sEPSC
g
Frequency (Hz)
100
10
1
Ctrl
FCD1
Ctrl
FCD1
sEPSC
sIPSC
h
Amplitude (pA)
100
10
**
Ctrl
FCD1
Ctrl
FCD1
sEPSC
sIPSC
i
Conductance (nS)
1
0.1
***
***
G_E,s
G_I,s
G_E,s
G_I,s
Control
FCD I
j
G_E,s/G_I,s
1.0
0.8
0.6
0.4
0.2
0.0
Ctrl
FCD1

Figure 2. Spontaneous synaptic inputs onto FSINs and PNs. (a) Representative traces of spontaneous excitatory and inhibitory postsynaptic currents (sEPSC and sIPSC) at FSINs. Scale bar, 25 pA (EPSC) or 100 pA (IPSC), 100 ms. **(b)** sEPSC (darker symbols), but not sIPSC (lighter symbols), frequency was higher in FCD I epilepsy (n = 34) compared to control (n = 38). For spontaneous events, two-sided unpaired t-tests were used. **(c)** sEPSC and sIPSC amplitudes were larger in FCD I epilepsy. sEPSC: control, 19.4 ± 1.3 (pA) (n = 38); FCD I, 25.7 ± 1.8 (pA) (n = 34). sIPSC: control, 19.3 ± 0.8 (pA) (n = 37); FCD I, 26.3 ± 2.4 (pA) (n = 34). **(d)** Spontaneous excitatory postsynaptic conductance ($G_{E,s}$) was smaller than spontaneous inhibitory postsynaptic conductance ($G_{I,s}$) at FSINs. Control: $G_{E,s}$ = 0.23 ± 0.02 (nS) (n = 38), $G_{I,s}$ = 0.39 ± 0.02 (nS) (n = 37); FCD I: $G_{E,s}$ = 0.30 ± 0.02 (nS) (n = 34), $G_{I,s}$ = 0.53 ± 0.05 (nS) (n = 34). **(e)** $G_{E,s}/G_{I,s}$ at FSINs favored inhibition, and was similar between control (0.59) and FCD I epilepsy (0.57). **(f)** Representative traces at PNs. Scale bar, 25 pA (EPSC) or 100 pA (IPSC), 100 ms. **(g)** sEPSC and sIPSC frequency was similar between control (n = 25) and FCD I epilepsy (n = 43). **(h)** sEPSC, but not sIPSC, amplitude was larger in FCD I epilepsy. sEPSC: control, 16.5 ± 0.7 (pA) (n = 25); FCD I, 21.0 ± 0.9 (pA) (n = 46). sIPSC: control, 23.2 ± 1.8 (pA) (n = 25); FCD I, 28.0 ± 1.7 (pA) (n = 43). **(i)** $G_{E,s}$ was smaller than $G_{I,s}$ at PNs. Control: $G_{E,s}$ = 0.19 ± 0.01 (nS) (n = 25), $G_{I,s}$ = 0.46 ± 0.04 (nS) (n = 25); FCD I: $G_{E,s}$ = 0.25 ± 0.01 (nS) (n = 46), $G_{I,s}$ = 0.56 ± 0.03 (nS) (n = 43). **(j)** $G_{E,s}/G_{I,s}$ at PNs further favored inhibition with a ratio lower than that at FSINs, and similar between control (0.42) and FCD I epilepsy (0.44). Source data are provided with this paper.

Figure 3

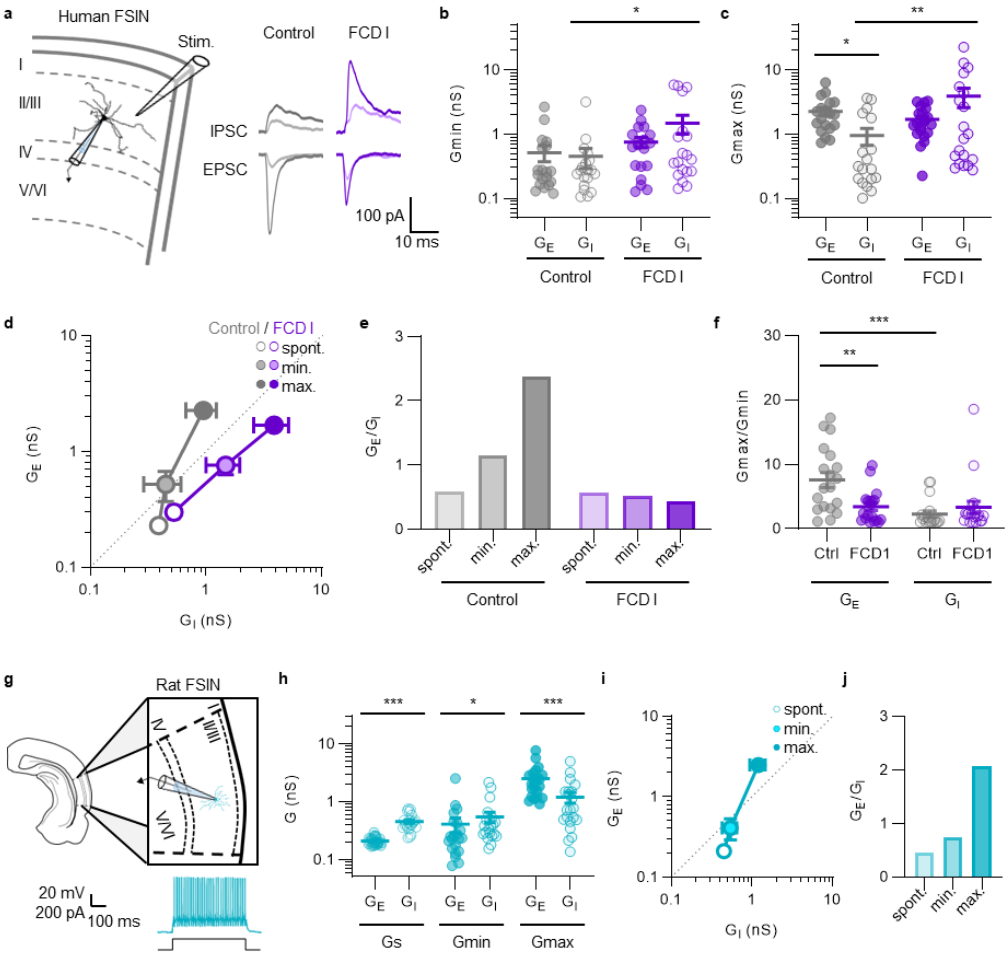
a
Human FSIN
Stim.
I
II/III
IV
V/VI
Control
FCD I
IPSC
EPSC
100 pA
10 ms
b
Gmin (nS)
Control
FCD I
c
Gmax (nS)
d
Control / FCD I
spont.
min.
max.
GE (nS)
GI (nS)
e
GE/GI
f
Gmax/Gmin
Ctrl
FCD1
g
Rat FSIN
20 mV
200 pA
100 ms
h
G (nS)
Gs
Gmin
Gmax
i
j

Figure 3. Net excitatory synaptic drive of FSINs scales with cortical activation, but is inverted towards inhibition in FCD I epilepsy. (a) Representative EPSC and IPSC at FSINs, evoked by minimal ($eEPSC_{min}$ and $eIPSC_{min}$; lighter traces) or maximal ($eEPSC_{max}$ and $eIPSC_{max}$; darker traces) stimulation. **(b)** Single excitatory synaptic conductance from minimal stimulation ($G_{E,min}$) was similar to single inhibitory conductance ($G_{I,min}$) at FSINs in both control and FCD I epilepsy. Control: $G_{E,min}$ = 0.52 ± 0.15 (nS) (n = 19), $G_{I,min}$ = 0.45 ± 0.16 (nS) (n = 19). FCD I: $G_{E,min}$ = 0.76 ± 0.13 (nS) (n = 19), $G_{I,min}$ = 1.48 ± 0.48 (nS) (n = 19). **(c)** Total excitatory synaptic conductance from maximal stimulation ($G_{E,max}$) was larger than total inhibitory conductance ($G_{I,min}$) at FSINs in control, but not FCD I epilepsy. Control: $G_{E,max}$ = 2.26 ± 0.33 (nS) (n = 19), $G_{I,max}$ = 0.95 ± 0.28 (nS) (n = 19); FCD I: $G_{E,max}$ = 1.69 ± 0.20 (nS) (n = 18), $G_{I,max}$ = 3.89 ± 1.30 (nS) (n = 20). **(d)** Excitatory vs. inhibitory synaptic conductances at FSINs (n = 37, 19, 19 (control), or 34, 19, 18 (FCD I); for G_s, G_{min}, and G_{max}). Net synaptic drive of FSINs progressively favored excitation in control, but this relationship was inverted towards inhibition in FCD I epilepsy. **(e)** G_E/G_I at FSINs progressively favored excitation in control, but not in FCD I epilepsy. **(f)** $G_{E,max}/G_{E,min}$ was larger than $G_{I,max}/G_{I,min}$ in control, but not in FCD I where $G_{E,max}/G_{E,min}$ was smaller compared to control and similar to $G_{I,max}/G_{I,min}$ (n = 19, 19 (G_E), or 18, 19 (GI); for control, FCD I). **(g)** Representative example of rat L2/3 FSIN (cyan). **(h)** Excitatory and inhibitory conductance, from spontaneous events (n = 22) or evoked by minimal (n = 21) or maximal (n = 21) stimulation. **(i)** Synaptic drive of rat FSINs scaled with cortical activation towards net excitation (n = 22, 21, 21; for G_s, G_{min}, and G_{max}). **(j)** G_E/G_I at rat FSINs increased progressively with cortical activation, similar to human FSINs in the non-epileptic control. Source data are provided with this paper.

913 **Figure 4**

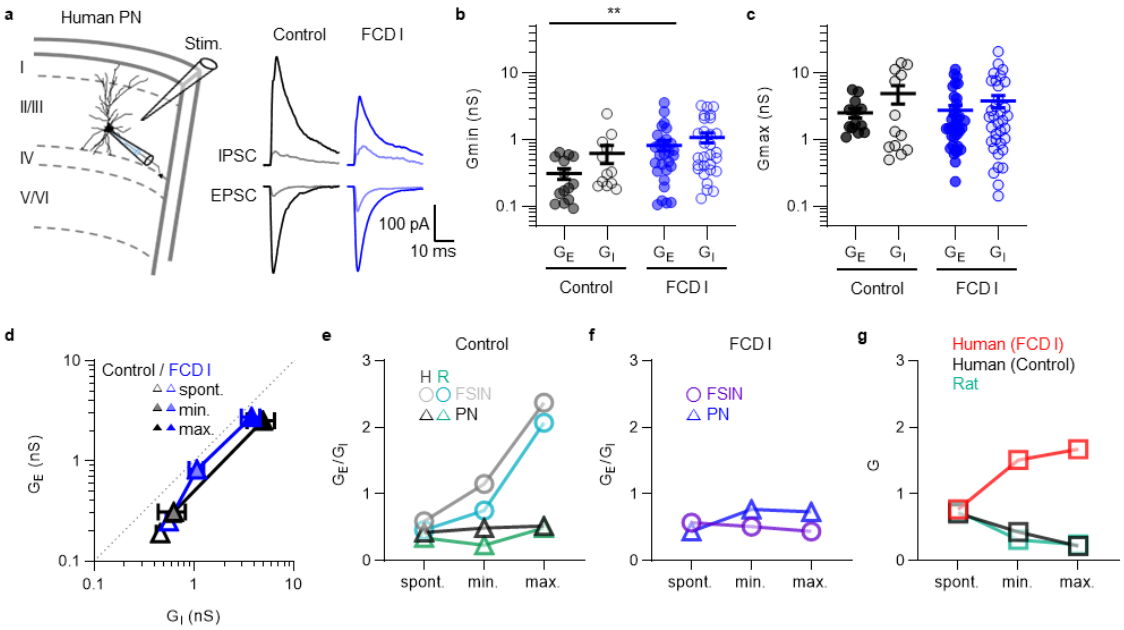

914

915

Figure 4. Monosynaptic conductances at PNs are unaffected in FCD I epilepsy. (a) Representative EPSC and IPSC traces at PNs. **(b)** $G_{E,min}$ was not significantly different from $G_{I,min}$ at PNs in both control and FCD I epilepsy. Control: $G_{E,min}$ = 0.31 ± 0.06 (nS) (n = 14), $G_{I,min}$ = 0.63 ± 0.19 (nS) (n = 12), P = 0.0757. FCD I: $G_{E,min}$ = 0.82 ± 0.14 (nS) (n = 29), $G_{I,min}$ = 1.07 ± 0.18 (nS) (n = 29), P = 0.4773. **(c)** $G_{E,max}$ was not significantly different from $G_{I,max}$ at PNs in both control and FCD I epilepsy. Control: $G_{E,max}$ = 2.52 ± 0.42 (nS) (n = 13), $G_{I,max}$ = 4.90 ± 1.49 (nS) (n = 13), P = 0.6866. FCD I: $G_{E,max}$ = 2.75 ± 0.48 (nS) (n = 35), $G_{I,max}$ = 3.78 ± 0.78 (nS) (n = 35), P = 0.6489. **(d)** Excitatory vs. inhibitory synaptic conductances at PNs, with different scales of cortical activation (n = 25, 12, 29 (control), or 43, 35, 35 (FCD I); for G_s, G_{min}, and G_{max}). Inhibition was always dominant over excitation at PNs in both control and FCD I epilepsy. **(e)** G_E/G_I at FSINs and PNs, from the human (H, gray and black) non-epileptic control or the rat (R, cyan and green) cortex. **(f)** G_E/G_I at FSINs and PNs, from human FCD I epilepsy. **(g)** Synaptic excitability variable $G = (G_{EE} \cdot G_{II})/(G_{EI} \cdot G_{IE})$, in human non-epileptic control (dark gray), human FCD I epilepsy (red), and the rat cortex (teal). Source data are provided with this paper.

932 **Figure 5**

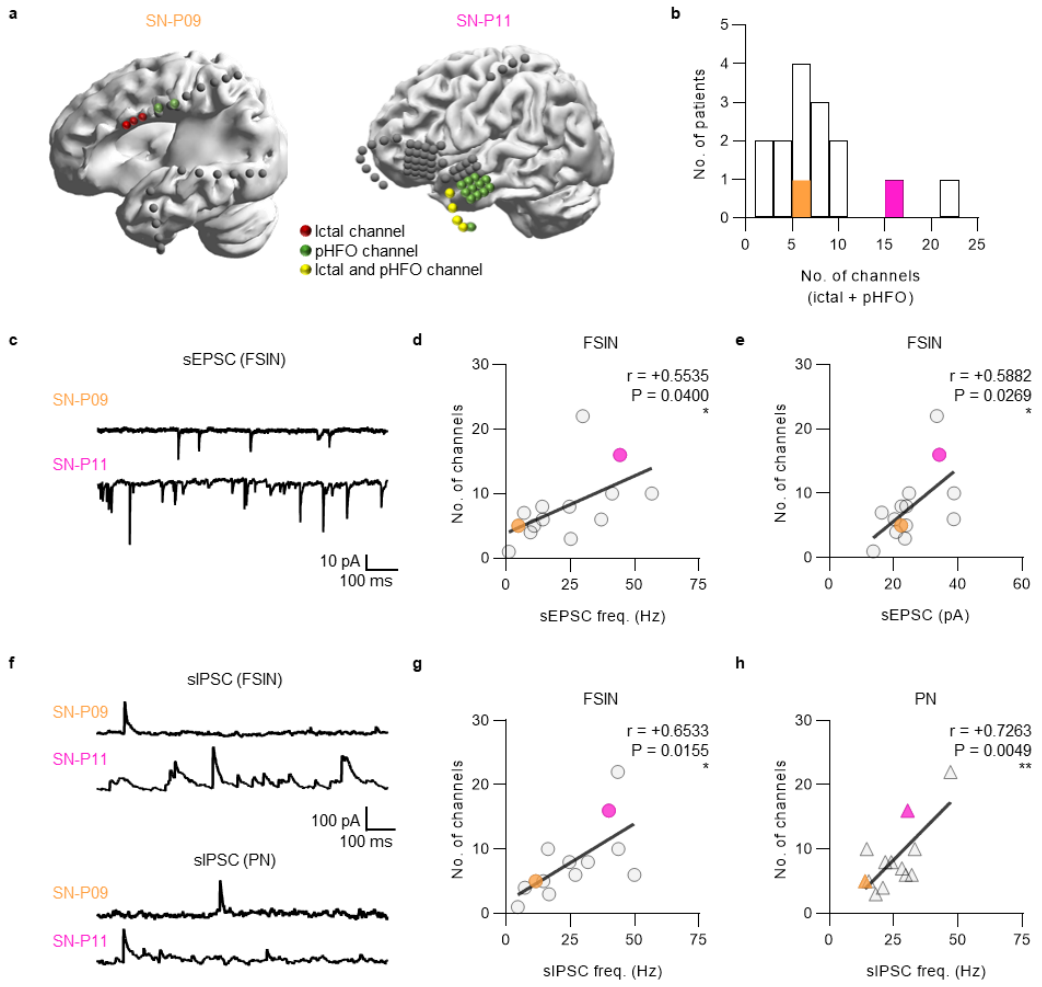

933

934

Figure 5. Cortical area exhibiting pathological activity in vivo is associated with spontaneous synaptic events at FSINs recorded ex vivo. (a) Representative examples of electrode locations from iEEG implants in two patients (labeled orange and pink). The spatial extent of cortical areas displaying pathological iEEG patterns (ictal/pHFO area) is represented by the number of channels displaying either ictal activity or pHFOs. Red, channels displaying ictal activity; green, channels displaying pHFOs; yellow, channels displaying both ictal activity and pHFOs. **(b)** Distribution of the number of channels corresponding to ictal/pHFO area across patients. **(c)** Representative traces of sEPSC at postsynaptic FSINs, recorded from slices obtained from the same patients shown in panel **a**. **(d)** Ictal/pHFO area in FCD I epilepsy was positively correlated with sEPSC frequency at postsynaptic FSINs ($r = +0.5535$, $P = 0.0400$). **(e)** Ictal/pHFO area was positively correlated with sEPSC amplitude at FSINs ($r = +0.5882$, $P = 0.0269$). **(f)** Representative traces of sIPSC at FSINs and PNs, from the same patients. **(g)** Ictal/pHFO area was positively correlated with sIPSC frequency at FSINs ($r = +0.6533$, $P = 0.0155$). **(h)** Ictal/pHFO area was positively correlated with sIPSC frequency at PNs ($r = +0.7263$, $P = 0.0049$). Source data are provided with this paper.

951 **Figure 6**

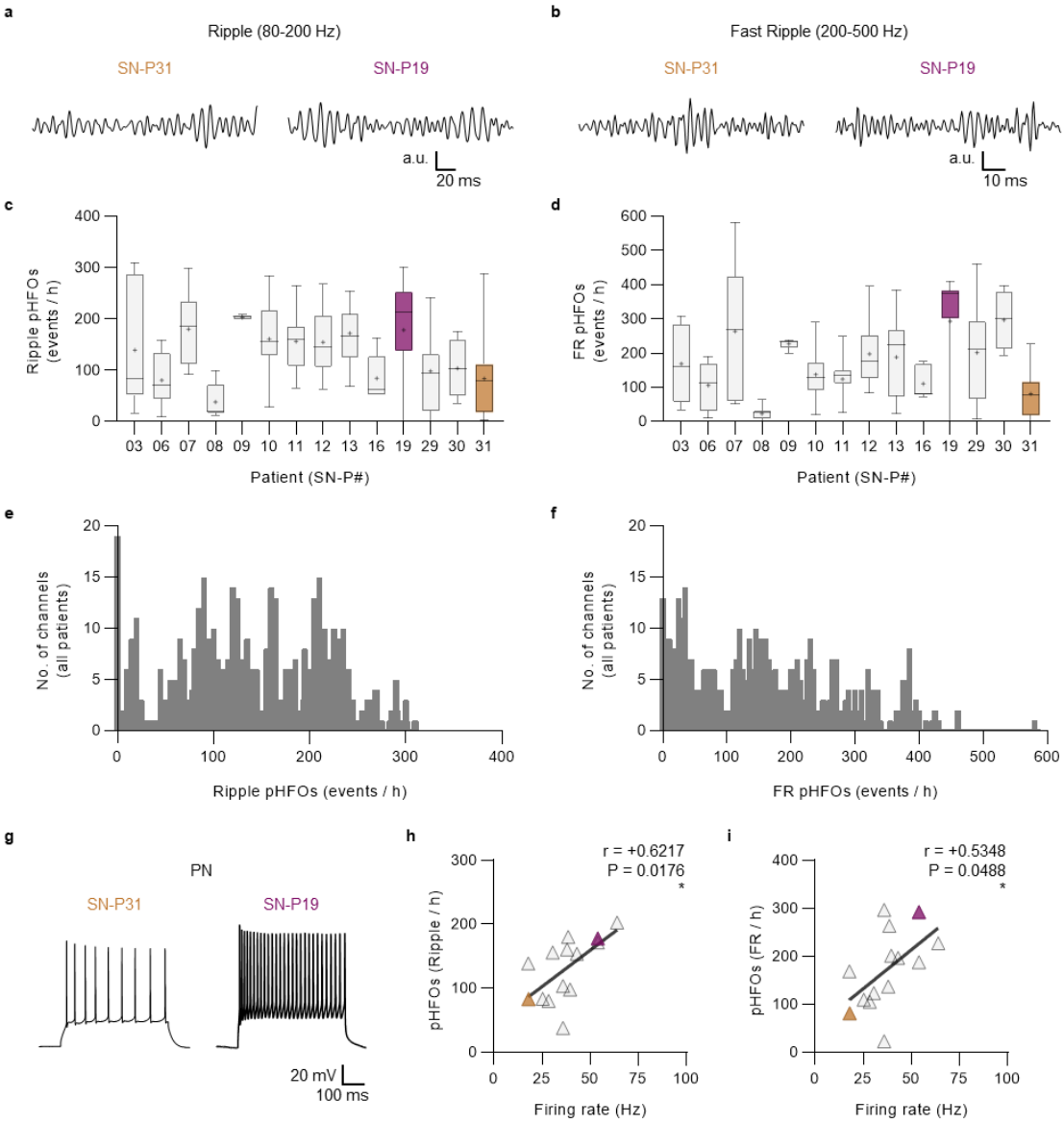

952

953

Figure 6. pHFO occurrence is associated with higher PN firing rate. (a) Representative examples of iEEG recordings displaying pHFOs at the ripple frequency range, from two patients (labeled brown and burgundy). **(b)** Representative iEEG recordings displaying pHFOs at the fast ripple frequency range, from the same patients shown in panel **a**. **(c)** Distribution of the number of ripple pHFO events observed within a 1-hour monitoring period, averaged across all pHFO-displaying channels, by each patient. The line across each box plot indicates the median, whereas the + sign indicates the mean. Box edges represent the 1st and 3rd quartiles, while the whiskers represent the minima and maxima. **(d)** Same as in panel **c**, but for fast ripple (FR) pHFO events. **(e)** Distribution of the number of ripple pHFO events per hour, from all channels irrespective of patient. **(f)** Distribution of the number of FR pHFOs per hour, from all channels irrespective of patient. **(g)** Representative traces of PN firing, recorded from slices obtained from the same patients shown in panels **a** and **b**. **(h)** The average number of ripple pHFO events observed per pHFO-displaying channel from the 1-hour monitoring period was positively correlated with PN firing rate ($r = +0.6217$, $P = 0.0176$). **(i)** Mean FR pHFOs per channel per hour was positively correlated with PN firing rate ($r = +0.5348$, $P = 0.0488$). Source data are provided with this paper.